

Modelling of tidally-induced hydro-sedimentary processes in the coastal zone of the southern part of the Dover Strait

Dover Strait
Tidal currents
Coastal sediments
Hydro-sedimentary processes
Modelling

Détroit du Pas-de-Calais
Courants de marée
Sédiments côtiers
Processus hydro-sédimentaires
Modélisation

Georges CHAPALAIN ^a, Hassan SMAOUI ^a, Alain LEPRETRE ^a, Kim Dan NGUYEN ^b, Abdellatif OUAHSINE ^b et Bernadette TESSIER ^c

^a Laboratoire d'Écologie Numérique, URA-CNRS 1363, Université des Sciences et Technologies de Lille, Bât. SN3, 59655 Villeneuve d'Ascq Cedex, France.

^b Laboratoire de Mécanique de Lille, URA-CNRS 1441, Université des Sciences et Technologies de Lille, Bât. M3, 59655 Villeneuve d'Ascq Cedex, France.

^c Laboratoire de Sédimentologie et Géodynamique, URA-CNRS 719, Université des Sciences et Technologies de Lille, Bât. SN5, 59655 Villeneuve d'Ascq Cedex, France.

ABSTRACT

The present paper deals with the modelling of hydro-sedimentary processes in the coastal area near Cape Gris-Nez and Cape Blanc-Nez (Dover Strait). The modelling procedure consists in coupling different hydro-sedimentary process models with a high spatial resolution two-dimensional tidal flow model (Nguyen and Ouahsine, 1992). The sediment transport models used include two semi-empirical models based on a dimensionless analysis and energetic concepts (Ackers and White, 1973; Engelund and Hansen, 1967), and a more heuristic *cu* (concentration times velocity) model (van Rijn, 1984 *a*; *b*). All these models are applied to predict instantaneous and tidally-integrated sediment transports in the area under investigation.

Oceanologica Acta, 1993. 16, 5-6, 517-529.

RÉSUMÉ

Modélisation des processus hydro-sédimentaires induits par la marée dans la zone côtière méridionale du détroit du Pas-de-Calais

Le présent article traite de la modélisation hydro-sédimentaire dans la zone côtière située aux abords du Cap Gris-Nez et du Cap Blanc-Nez (détroit du Pas-de-Calais). La démarche consiste à interfacier divers modèles de processus hydro-sédimentaires avec un modèle numérique bidimensionnel à haute résolution spatiale des courants de marée (Nguyen et Ouahsine, 1992). Parmi les modèles de transport sédimentaire utilisés, on en compte deux semi-empiriques basés sur une analyse dimensionnelle et des concepts énergétiques (Ackers and White, 1973 ; Engelund et Hansen, 1967) et un modèle plus heuristique de type *cu* (calculant le transport sédimentaire instantané sur la base du produit d'une concentration en sédiment par une vitesse d'advection; van Rijn, 1984 *a* ; *b*). Ces modèles sont appliqués pour calculer les transports sédimentaires instantanés, puis intégrés sur un cycle de marée dans la zone d'étude.

Oceanologica Acta, 1993. 16, 5-6, 517-529.

INTRODUCTION

For several decades, the southern coast of the Dover Strait has been subjected to intense perturbations due to human activity development (port facilities construction, dredging, granulate extraction, *etc.*). The impact of these pressures has been accentuated by additional perturbations like remote disturbances in rivers that are sources of coastal sediments, and long-term phenomena such as the variation of the mean sea-level and storm conditions.

Under the ambient macrotidal hydrodynamic conditions, all these perturbations result in progressive modifications of the sea-bed with repercussions as far as the coastline. A better understanding of these interactions between the fluid in motion and the sea-bed on which it flows, as well as the elaboration of eventual control and protection plans, depend in great measure on predictive and deterministic modelling based on the principles of the physical sciences.

The subject of this paper is the development of such modelling and its application to the coastal boundary zone including Cape Gris-Nez and Cape Blanc-Nez (Fig. 1). Among the hydrodynamic driving forces, only tides are taken into account here. A further stage in the investigation will deal with the inclusion of wave effects. In a series of geographical locations which were subject to a surficial sediment sampling, the hydro-sedimentary modelling procedure consists in the coupling of different submodels of grain-related roughness, skin shear stress, incipient movement and suspension, bedform generation, overall bed roughness and sediment transport rate with a high resolution two-dimensional numerical model of tidal currents. Before focusing on the different steps of the modelling procedure, we shall present specific and general data concerning the study area.

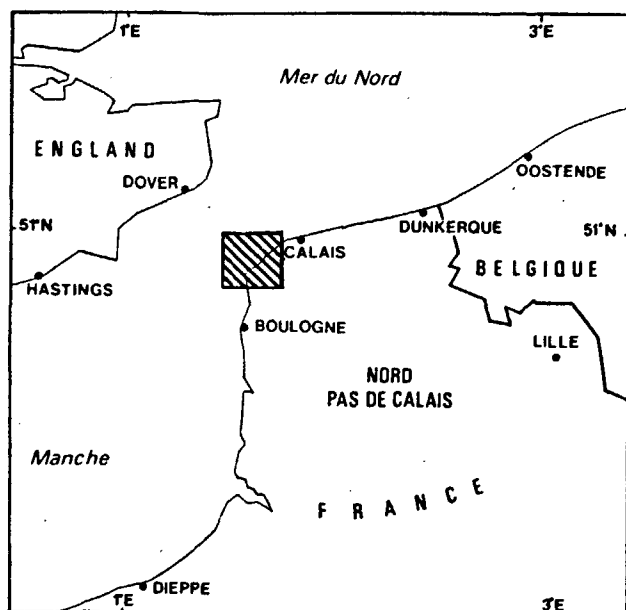


Figure 1
Location of the study area.
Localisation de la zone d'étude.

DATA CONCERNING THE SOUTHERN PART OF THE DOVER STRAIT

The area under investigation is characterized by moderate bottom slopes and a maximum depth of about 35 m (Fig. 2). The spatial distribution of surficial sediments established in 1985 by Augris *et al.* (1987 *a; b*) is summarized in Figure 3. It shows four zones:

- a sector of fine and medium sands situated near the coastline. This sector is characterized between Cape Gris-Nez and Cape Blanc-Nez by a sandy banner bank named Banc à la Ligne, the top of which reaches its highest point at 1m below the hydrographical zero (Fig. 2). This large

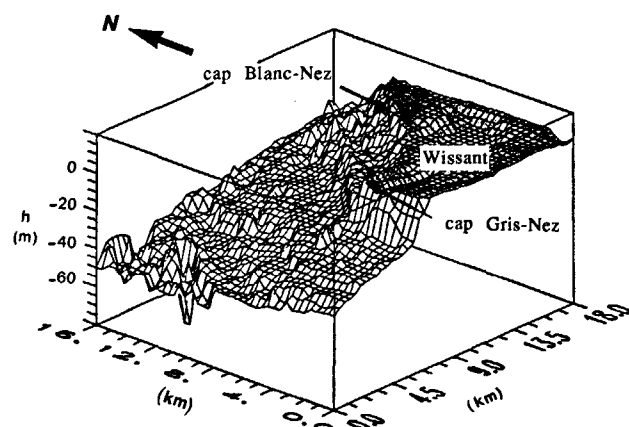


Figure 2
Bathymetry of the study area.
Bathymétrie de la zone d'étude.

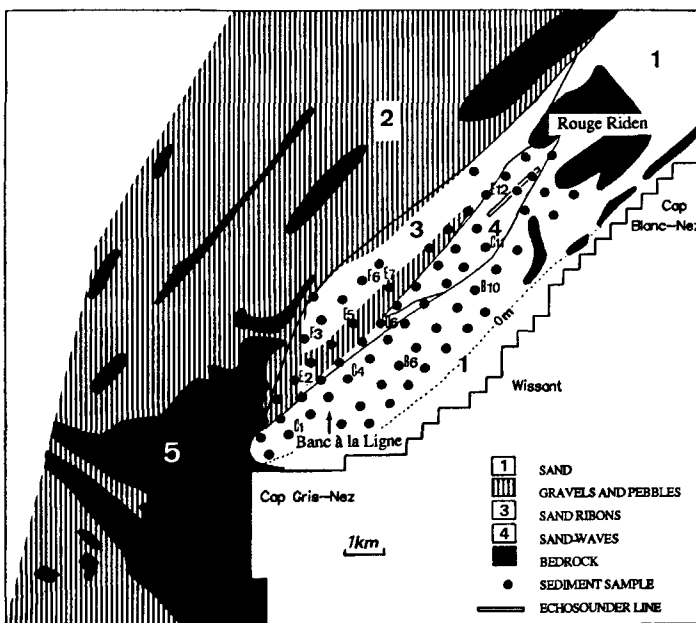
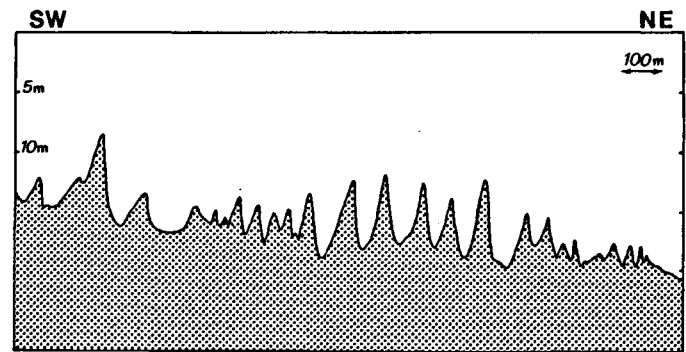


Figure 3
Simplified surficial sediments map (after Augris *et al.*, 1987 *a; b*) with the locations of sediment samples and echosounder recording line presented on Figure 4.
Cartographie simplifiée des sédiments superficiels (d'après Augris *et al.*, 1987) et localisation des douze points sélectionnés à travers la zone d'étude et du transect d'échosondage.

Figure 4

Echosounder recording line across the subsector of sand-waves.

Transect d'échosondage dans le sous-secteur de vagues de sable.



sedimentary structure, 3.5 km long and 2 km wide, is aligned SW-NE and almost connected with the coastline near Cape Gris-Nez. Its relief decreases in the northeastern direction to vanish off Cape Blanc-Nez. Ripples less than 5 cm high appear throughout the sector (Augris *et al.*, 1990);

- a gravel (2 mm to 2 cm) and pebble (> 2 cm) sector located offshore. This substrate is made of a terrigenous material comprising flint and rock fragments of local origin (limestone or sandstone) and a biogenic component made of more or less broken skeletons of invertebrates and shells (Augris *et al.*, 1990);

- an intermediate sector situated between the two previous sectors and itself divided into a subsector of sand ribbons and furrows next to the outer gravel and pebble sector, and a subsector of sand-waves close to the inner sandy sector (Fig. 4);

- isolated rocky outcrops located essentially off Cape Gris-Nez where they exhibit bars with a strong relief in the WNW-ESE direction, and to the northeast of Cape Blanc-Nez (Rouge Riden area).

A surficial sediment sampling campaign was carried out in January 1992 using a van Veen grab. A total of 67 samples were taken (Fig. 3). The longshore spacing between samples was 500 m and the cross-shore spacing varied from 400 to 600 m. The principal characteristics of the bottom sediment pattern observed by Augris *et al.* (1987 *a*; *b*) are confirmed. A close examination of selected samples, the grain-size frequency distributions of which are presented on Figure 5, reveals the heterogeneity of the sediments in the intermediate sector between the offshore gravelly sector and the inner sandy sector. Between Wissant and Cape Blanc-Nez, close to the Rouge Riden area, a sample contains a large amount of mud (more than 71 % of the total mass are smaller than 63 μm). Due to the lack of information about the grain-size frequency distribution of these fine fractions and the very specific hydro-sedimentary behavior of this kind of sediments, this sample was eliminated.

From a hydrodynamic point of view, the southern part of the Dover Strait area is a semidiurnal macrotidal environment characterized by a mean spring tidal range exceeding 6 m and strong currents which can exceed 1.8 m s^{-1} . Several two-dimensional horizontal models solving numerically the tidal wave propagation were undertaken on the study area (*e.g.*, Werner and Lynch, 1987; Salomon and Breton, 1991; Nguyen and Ouahsine, 1992). In this paper, we shall use the results of the finite-

difference model developed by Nguyen and Ouahsine (1992). This model has a spatial resolution of 500 m descending to 250 m in the western part of the study area. It is forced by 29 tidal harmonic components. Figure 6 shows, for instance, the calculated instantaneous depth-integrated current field fifteen minutes after high tide at Calais for a mean tide (*i.e.*, tide coefficient 70). Moreover, it must be noted that the Eulerian residual flow exhibits a lee eddy in the western part of Wissant Bay (Nguyen and Ouahsine, 1992).

MODELLING OF HYDRO-SEDIMENTARY PROCESSES

Preliminary aspects

Modelling of hydro-sedimentary processes is undertaken at the different geographical locations where grain-size data are available (Fig. 3). This work requires a preliminary integration of local information concerning:

- the surficial sediment texture and the bed configuration: this stage consists in integrating on one hand the granulometric data *via* a series of position diameters corresponding to different fractions: d_{16} (grain size for which 16 % by weight of the sample is finer), d_{35} , d_{50} , d_{65} , d_{84} , d_{90} ; on the other hand a flag connected with the spatial sectorization (sandy sector, sand ribbons and furrows subsector, sand-wave subsectors) in order to take it into account in the calculation of local sedimentological and morphodynamical particularities. Notice that we have truncated the grain-size distributions (> 2.5 mm) for the samples collected in the intermediate sand ribbons and furrows subsector. These coarse fractions correspond in part to broken shells which exhibit a very specific mechanical behaviour during transportation relative to sandy sediments. Part of these fractions also comprises gravels. In this case, the truncation procedure may be justified by the fact that elements of these fractions originate from the underlying gravel and pebble layer reached during sampling, and are not actually involved in transportation processes;

- instantaneous tidal flow characteristics, namely water-depth h and depth-averaged velocity \bar{u} issued from the numerical tidal model. In the shallow waters of the study area, the veering effects caused by the Earth's

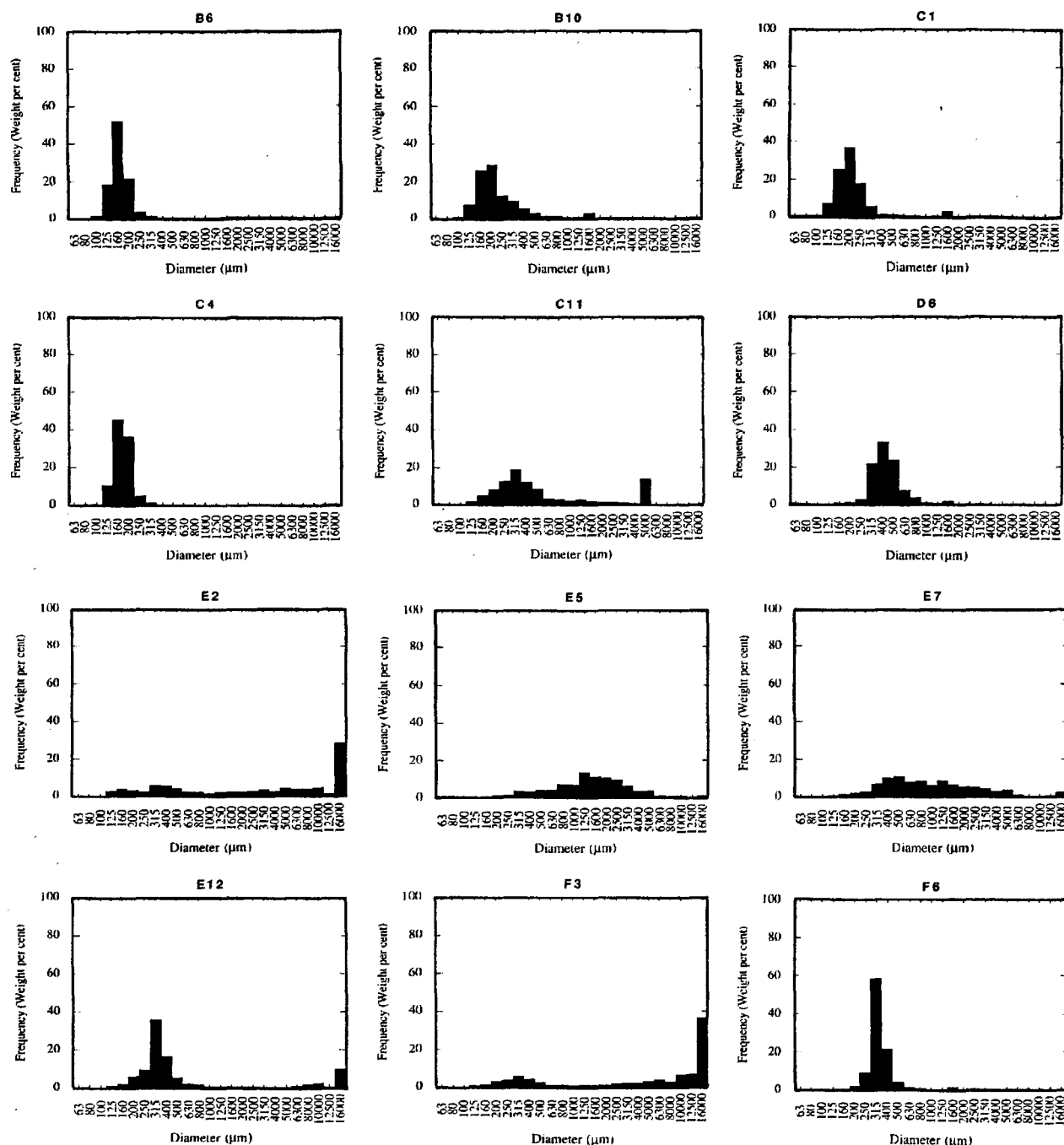


Figure 5

Grain-size frequency distributions at the twelve sites selected on Figure 3.

Distributions granulométriques des échantillons collectés aux douze points sélectionnés à la figure 3.

rotation in the bottom boundary layer are neglected. This stage goes through a bilinear interpolation of flow characteristics computed at the four nodes of the numerical grid containing the surficial sediment sample location where hydro-sedimentary processes will be modelled.

Modelling aspects

The hydro-sedimentary modelling is largely based on van Rijn's (1984 *a; b*; 1989) works. The successive steps of the modelling procedure are now examined.

Calculation of the grain-related roughness height

The grain-related roughness height k'_s is usually assumed to be directly proportional to a position diameter. Some expressions are given in Table 1. The results of the application of these different models in a series of sites selected in the study area and displayed on Figure 3 are presented in Table 2. The lower values of the grain-related roughness height are observed in the inner western part of Wissant Bay where sediments are fine. The higher values of the grain-related roughness height are found in the intermediate sector characterized by coarser sediments.

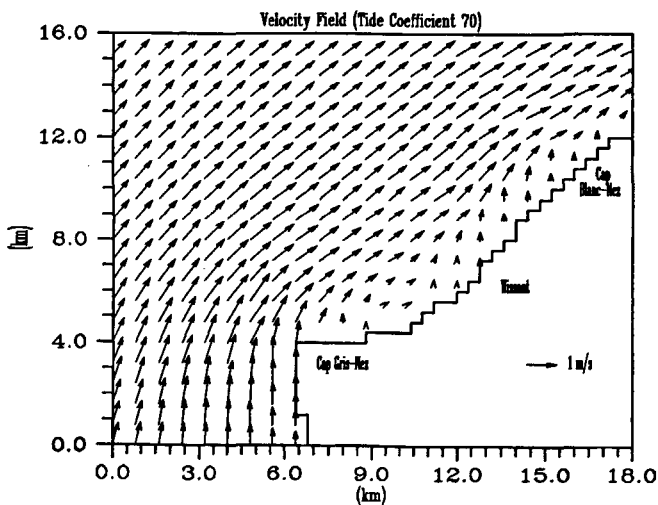


Figure 6

Computed tidal velocity field [15 mn after high tide at Calais for a mean tide (after Nguyen and Ouahsine, 1992)].

Champ des courants instantanés calculés à Pleine Mer à Calais + 15 mn pour une marée moyenne (d'après Nguyen et Ouahsine, 1992).

site	sector code	Engelund & Hansen's model	Ackers & White's model	van Rijn's model
B6	1	0.39	0.21	0.72
B10	1	0.52	0.25	1.47
C1	1	0.49	0.25	1.02
C4	1	0.42	0.23	0.74
C11	4	0.89	0.39	2.71
D6	3	1.04	0.53	2.24
E2	3	1.06	0.40	4.00
E5	3	2.70	1.02	5.36
E7	3	1.80	0.64	4.72
E12	3	0.79	0.42	1.72
F3	3	0.93	0.38	3.49
F6	3	0.79	0.44	1.48

Calculation of the grain-related shear stress

A turbulent flow on a rough bottom yields a fluid velocity profile given by the following von Karman-Prandtl equation:

$$u = \frac{u_*}{k} \ln \left(\frac{z}{k'_s/30} \right) \quad (1)$$

in which k is von Karman constant equal to 0.4, z is the height above the bottom and u_* is the friction velocity. u_* is connected to the grain-related shear stress by the relation $u_* = \sqrt{\tau'_b/\rho}$ in which ρ is the water specific gravity equal to 1000 kg m^{-3} .

It follows that the skin shear stress τ'_b exerted on grains may be expressed in terms of the grain-related roughness height k'_s , the water-depth h , and the depth-averaged velocity \bar{u} by:

$$\tau'_b = 0.16 \rho \ln^{-2} (11 h/k'_s) \bar{u}^2 \quad (2)$$

Note that the factor 11 in equation (2) is commonly replaced by 12 in Dutch papers (e.g. van Rijn, 1981; 1982;

1984 a; b; c; 1989).

Skin shear stresses predicted at the different selected sites by the previous three grain-related roughness height models for the instantaneous flow field displayed on Figure 6 are tabulated in Table 3. We notice a slight sensitivity of skin shear stresses to grain-related roughness height models.

Quantification of the initiation of sediment transport

Two modes of transport are generally considered: on one hand the bedload transport at and near the bottom

Table 1

Grain-related roughness height models.

Modèles de hauteur de rugosité liée aux grains.

Engelund and Hansen's (1967) model	$k'_s = 2 d_{65}$
Ackers and White's (1973) model	$k'_s = 1.25 d_{35}$
van Rijn's (1982) model	$k'_s = 3 d_{90}$

Table 2

Grain-related roughness height (in millimetres) predicted at different sites by models of Engelund and Hansen (1967), Ackers and White (1973) and van Rijn (1982). The second column indicates the code of sector or subsector in which the site is located. This code is presented in Figure 3.

Hauteur de rugosité liée aux grains (en millimètres) prédite aux différents points par les modèles de Engelund et Hansen (1967), Ackers et White (1973), van Rijn (1982). La deuxième colonne indique le code du secteur dans lequel se trouve le point. Ce code est explicité à la figure 3.

including saltation; on the other hand the suspended load transport. With regard to transport process initiation, we investigate both modes by presenting succinctly van Rijn's (1981; 1984 a; b; 1989) works.

• Bedload case

When the driving force moment (proportional to the skin shear stress and the sediment particle surface) becomes higher than the resistant force moment (related to the particle immersed weight) an initiation of particle motion occurs. That result is usually presented in a form involving the well-known Shields' (1936) coefficient θ :

$$\theta = \tau'_b / [(\rho_s - \rho) g d_{50}] \geq \theta_{cr} = \tau'_{b cr} / [(\rho_s - \rho) g d_{50}] \quad (3)$$

where g is the acceleration due to gravity, ρ_s is the sediment specific gravity equal to 2650 kg m^{-3} for a quartz sand, $\tau'_{b cr}$ and θ_{cr} are respectively the threshold values of the skin shear stress and Shields coefficient often experimentally given in terms of the Reynolds number $Re = u_* d/\nu$ where ν is the water molecular viscosity equal to $10^{-6} \text{ m}^2 \text{ s}^{-1}$. Van Rijn (1981; 1989) suggests the following

Table 3

Skin shear stress (in $N m^{-2}$) predicted at different sites by models of Engelund and Hansen (1967), Ackers and White (1973) and van Rijn (1982), and effective current-related shear stress predicted by van Rijn's (1982) model.

Contrainte de cisaillement exercée sur les particules (en $N m^{-2}$) calculée aux différents points à l'aide des modèles de Engelund et Hansen (1967), Ackers et White (1973), van Rijn (1982), et contrainte de cisaillement globale calculée à l'aide du modèle de van Rijn (1982).

site	Skin shear stress (Engelund & Hansen's model)	Skin shear stress (Ackers & White's model)	Skin shear stress (van Rijn's model)	Effective shear stress (van Rijn's model)
B6	0.12483	0.11382	0.13605	0.30020
B10	0.30456	0.27224	0.35761	0.73119
C1	0.32618	0.29342	0.36490	0.82105
C4	0.23731	0.21473	0.25666	0.58470
C11	0.73334	0.64374	0.87535	1.94032
D6	0.39204	0.35074	0.44064	0.99246
E2	0.48716	0.41831	0.60297	1.15820
E5	0.56258	0.47599	0.62757	1.48203
E7	0.58619	0.49509	0.68445	1.43039
E12	1.06045	0.96070	1.18686	2.56085
F3	0.63940	0.55842	0.78738	1.50044
F6	0.52744	0.48193	0.57558	1.25293

expression for the Shields empirical curve:

$$\begin{cases} \theta_{cr} = 0.24 d_*^{-1} & 1 < d_* \leq 4 & (4 a) \\ \theta_{cr} = 0.14 d_*^{-0.64} & 4 < d_* \leq 10 & (4 b) \\ \theta_{cr} = 0.04 d_*^{-0.1} & 10 < d_* \leq 20 & (4 c) \\ \theta_{cr} = 0.013 d_*^{0.29} & 20 < d_* \leq 150 & (4 d) \\ \theta_{cr} = 0.055 & d_* > 150 & (4 e) \end{cases}$$

in which:

$$d_* = [(s-1)g/v^2]^{1/3} d_{50} \quad (5)$$

$$s = \rho_s/\rho \quad (6)$$

• Suspended load case

Sediment particles remain in suspension, and suspended load transport may occur, as long as the upward contribution of turbulent vertical velocity fluctuations, which can be represented by the vertical turbulence intensity, exceeds the downward contribution due to their fall velocity w_f expressed by van Rijn as:

$$w_f = \frac{(s-1)g d_s^2}{18\nu} \quad 1 < d_s < 100 \mu m \quad (7 a)$$

$$w_f = \frac{10}{d_s} \left[\left(1 + \frac{(s-1)g d_s^3}{\nu^2}\right)^{0.5} - 1 \right] \quad 100 \leq d_s \leq 1000 \mu m \quad (7 b)$$

$$w_f = 1.1 [(s-1)g d_s]^{0.5} \quad d_s > 1000 \mu m \quad (7 c)$$

where d_s is a specific diameter of suspension given by:

$$d_s = d_{50} [1 + 0.011 (\sigma_s - 1) (T - 25)] \quad (8)$$

with:

$$\sigma_s = 0.5 (d_{50}/d_{16} + d_{84}/d_{50}) \quad (9)$$

Table 4

Sets of constants in the ripple-related roughness height model (equation 15).

Différents jeux de constantes intervenant dans le modèle de hauteur de rugosité liée aux rides.

	A	B
Shinohara and Tsubaki's (1959) model	7.5	0.57
Wooding <i>et al.</i> 's (1973) model	60	1.4
van Rijn's (1982) model	20	1

$$T = (\tau'_b - \tau'_{b cr})/\tau'_{b cr} \quad (10)$$

The combination of three different formulations for the fall velocity is a means of taking as much account as possible of the heterogeneity of sediments.

By considering that the value of the vertical turbulence intensity is of the same order of magnitude as the friction velocity u_* (see Hinze, 1959; Kreplin and Eckelman, 1979) the threshold criterion of suspension (Middleton, 1976) can be given by:

$$u_{*cr} s/w_f = 1 \quad (11)$$

On an experimental basis, Bagnold (1956) and Engelund (1965) suggested replacing the constant unity respectively by 0.8 and 0.25. More recently, van Rijn (1984 *b*) proposed a variant to this type of criteria:

$$u_{*cr} s/w_f = 4/d_* \quad 1 < d_* \leq 10 \quad (12 a)$$

$$u_{*cr} s/w_f = 0.4 \quad d_* > 10 \quad (12 b)$$

Note that Ackers and White (1973) proposed an initiation criterion of the total load transport which will be presented during the formulation of their sediment transport model [see section "Calculation of the instantaneous sediment transport rate"].

Calculation of the overall bed roughness height

Following van Rijn (1989), the overall bed roughness height k_{sc} is expressed as the summation of the form and the particle roughness heights (see also O'Connor, 1991). Let us now examine the different contributions to the form roughness height.

• Contribution related to ripples

The roughness height related to ripples k_{sr} is usually expressed in terms of ripple wave-length λ_r and ripple height h_r . Firstly, those geometrical parameters are calculated by using empirical models originally proposed by Allen (1963), Yalin (1985) and van Rijn (1989, personal communication):

$$\lambda_r = 1000 d_{50} \quad (13)$$

$$h_r = 100 d_{50} \quad (14)$$

Secondly, the roughness height related to ripples k_{sr} is expressed in the form:

$$k_{sr} = A h_r (h_r/\lambda_r)^B \quad (15)$$

where A and B are constants.

Different sets of values are available in the literature. Some of them are given in Table 4. Later, we shall arbitrarily choose the van Rijn's (1982) relationship. On account of equations (13) and (14), this model reduces to:

$$k_{sr} = 200 d_{50} \quad (16)$$

• Contribution related to sand-waves

The roughness height connected with sand-waves k_{sw} is predicted by the van Rijn's (1989) empirical model:

$$k_{sw} = 1.1 \gamma_d \Delta_d [1 - \exp(-25 \Delta_d / \lambda_d)] \quad (17)$$

where Δ_d and λ_d are respectively the height and the length of sand-waves and γ_d is an empirical function of the slope of the lee side of sand-waves (see van Rijn, 1989, Fig. 7.2.3). The values of those parameters are extracted from echo-sounder observations carried out in February 1992 (Fig. 4). The ranges of these values are given on Table 5. The use of this model, derived from one-dimensional laboratory and field data, is allowed by the rectilinearity of tidal currents in the sand-waves subsector.

The different contributions to the roughness height calculated at the selected sites for the above chosen tidal flow field are given in Table 6. Contributions related to grain-size and ripple structures are computed on the basis of all the van Rijn's (1982) relationships. The different contributions are all maximum in the intermediate sector between the inner sandy sector and the offshore gravel and pebble sector. The contribution related to ripples is 20 to 50 times higher than the contribution related to grains. In the sand-waves subsector, the contribution of these features to the overall bed roughness height is significant with a maximum value reaching 3.12 m.

Table 5

Ranges of sand-wave parameters observed in the study area.

Gamme des valeurs des paramètres caractérisant les vagues de sable dans la zone d'étude.

	minimum value	maximum value
Sand wave height: Δ_d (m)	2	5
Sand wave length: λ_d (m)	75	200
Lee side length: λ_1 / Δ_d	5	10
λ_1 / λ_d	1/3	2/3

site	grain-related roughness height	ripple-related roughness height	sand-wave-related roughness height	total roughness height
B6	0.72	36.6	0.	37.3
B10	1.47	45.4	0.	46.9
C1	1.02	44.6	0.	45.6
C4	0.74	38.8	0.	39.5
C11	2.71	74.0	26.5	103.2
D6	2.24	93.4	0.	95.6
E2	4.00	82.0	0.	86.0
E5	5.36	215.0	0.	220.4
E7	4.72	131.0	0.	135.7
E12	1.72	73.4	0.	75.1
F3	3.49	74.8	0.	78.3
F6	1.48	74.2	0.	75.7

Table 6

Different contributions to the roughness height (in mm) at different sites.

Différentes contributions à la hauteur de rugosité (en millimètres) aux différents points.

Calculation of the effective current-related bed shear stress and friction velocity

Assuming a hydrodynamically rough flow yields the following expressions for the effective current-related bed shear stress τ_b and friction velocity u_*c :

$$\tau_b = 0.16 \rho \ln^{-2} (11 h/k_{sc}) \bar{u}^2 \quad (18)$$

$$u_*c = 0.4 \ln^{-1} (11 h/k_{sc}) \bar{u} \quad (19)$$

where:

$$k_{sc} = k'_s + k_{sr} + k_{sw} \quad (20)$$

The values of the effective current-related bed shear stress calculated at the selected sites for the chosen flow field are tabulated in Table 3. They exhibit a significant variability. The entire set of values indicates on one hand a cross-shore gradient in the southwest sector between Cape Gris-Nez and Wissant, on the other hand a homogeneity in the northeast sector between Wissant and Cape Blanc-Nez.

Calculation of the instantaneous sediment transport rate

Numerous models are available to predict sediment transport rates (see Raudkivi, 1976; Sleath, 1984; Dyer, 1986; van Rijn, 1984 a; b; 1989). A classification of these models permits a distinction between, on the one hand, experimental models (e.g. Meyer-Peter and Müller, 1948), and on the other hand semi-empirical models that are of two kinds: "theoretical" models based only on physical concepts; and other models based also on dimensionless analysis (e.g. Engelund and Hansen, 1967; Ackers and White, 1973). The "theoretical" models themselves fall into three basic subgroups: 1) *cu* models which consider the sediment transport rate as the product of the sediment concentration times the sediment velocity (van Rijn, 1984 a; b); 2) particle trajectory models which integrate the pick-up function concept in a probabilist (Einstein, 1950) or deterministic (van Rijn,

1984 *c*; 1986) manner; 3) energetic models based on the work done by the flow in moving sediment grains (Bagnold, 1966). Comparison of all these models with laboratory and field experiments shows that models by van Rijn (1984 *a*; *b*), Ackers and White (1973) and Engelund and Hansen (1967) are the most reliable (White *et al.*, 1975; van Rijn, 1984 *a*; *b*). Van Rijn's (1984 *a*; *b*) model yields the best result with predicted rates within a factor two of the measured rate in 76 % of the cases. Ackers and White's (1973) and Engelund and Hansen's (1967) models are less accurate, with a score of 68 and 63 %, respectively. Bagnold's (1966) model reaches the poor result of 22 % in the comparative study made by White *et al.* (1975). As a consequence, we shall here only present and apply Ackers and White's (1973), Engelund and Hansen's (1967) and van Rijn's (1984 *a*; *b*; 1989) models.

Notice that these models can only represent the transport of particles issued from local bottom sediments. In no case can they account for suspension transport of fine particles picked up elsewhere. This restriction is not very constraining in the essentially sandy environment characterizing the study area.

All the transport rate relationships presented below will be related to a volumetric transport per width unity; they will therefore be expressed in $m^2 s^{-1}$. They will provide the modulus of the instantaneous sediment transport vectors that will have the orientation of the instantaneous depth-averaged tidal current vectors.

• Ackers and White's (1973) model

On the basis of 925 laboratory and field experiments, Ackers and White (1973) proposed the following total transport rate equation:

$$q = K \bar{u} d_{35} \left(\frac{\bar{u}}{u_{*c}} \right)^n \left(\frac{Y - Y_{cr}}{Y_{cr}} \right)^m \quad (21)$$

where Y is the mobility parameter expressed as:

$$Y = \frac{u_{*c}^n}{[(s-1)g d_{35}]^{0.5}} \left(\frac{\bar{u}}{2.46 \ln(10 h/d_{35})} \right)^{1-n}$$

and the critical value Y_{cr} , as well as constants K , n and m , depends on d_* (equation 5):

for $d_* < 60$

$$K = \exp [2.86 \ln(d_*) - 0.434 \ln^2(d_*) - 8.13]$$

$$Y_{cr} = \frac{0.23}{d_{35}^{0.5}} + 0.14$$

$$n = 1 - 0.243 \ln(d_*)$$

$$m = \frac{9.66}{d_*} + 1.34 \quad (23)$$

and for $d_* \geq 60$

$$K = 0.025$$

$$Y_{cr} = 0.17$$

$$n = 0$$

$$m = 1.5$$

$$\quad (24)$$

This equation is valid for $40 \mu m < d_{50} < 4000 \mu m$.

• Engelund and Hansen's (1967) model

Based on energetic considerations, Engelund and Hansen (1967) developed the following expression for the total transport rate:

$$q = \frac{0.05 \bar{u}^5}{(s-1)^2 g^{0.5} d_{50} [7.83 \ln(11 h/k_{sc})]^3} \quad (25)$$

The calibration constant in equation (25) is produced by compiling about one hundred laboratory experiments. Moreover, it should be noted that this model does not incorporate a threshold condition, so that transport occurs even at small flow velocity.

• Van Rijn's (1984 *a*; *b*) model

In van Rijn's model (1984 *a*; *b*) both components of the transport - *i.e.* bedload and suspended load - are calculated separately before summation in order to find the total transport rate.

Van Rijn (1984 *a*) expressed the bedload transport rate as:

$$q_b = \delta_b c_b u_b \quad (26)$$

where δ_b , c_b and u_b are respectively the saltation height, the bedload concentration and the velocity of sediment particles.

By solving the equations of particle movement and using experimental data, van Rijn (1984 *a*) estimated δ_b and u_b by:

$$\frac{\delta_b}{d} = 0.3 d_*^{1.7} T^{0.5} \quad (27)$$

$$u_b = 1.5 [(s-1)g d_{50}]^{0.5} T^{0.6} \quad (28)$$

Using equation (26) with, on the one hand, theoretical results for bedload height and particle velocity and, on the other hand, sediment transport measurements, van Rijn (1984 *a*) obtained an expression for bedload concentration c_b in the form:

$$c_b = 0.18 c_0 \frac{T}{d_*} \quad (29)$$

where c_0 is the maximal concentration of substratum equal to 0.65.

The integration of previous elements (equations 26-29) leads, for sediment grains sized from 200 to 2000 μm to the following expression for the bedload transport rate (van Rijn, 1984 *a*):

$$q_b = 0.053 [(s-1)g]^{0.5} d_{50}^{1.5} d_*^{-0.3} T^{2.1} \quad (30)$$

The suspended load transport rate is given by:

$$q_s = \int_{k_s}^h c u dz \quad (31)$$

where the reference level is applied at the overall bed roughness height (van Rijn, 1984 *a*).

In agreement with equations (18) and (19), the fluid velocity profile is taken of the form:

$$u = \frac{u_{*c}}{k} \ln \left(\frac{z}{k_{sc}/30} \right) \quad (32)$$

This logarithmic profile is not a convenient approximation to the velocity distribution near the surface, but it does

provide a good and workable model in the lower part of the water column where most of sediment transport occurs.

The concentration profile is obtained by solving the vertical advection/dispersion equation in which van Rijn (1984 b) considers a parabolic eddy diffusivity profile in the lower half of the water column and constant in the higher half:

$$\frac{c}{c_a} = \left(\frac{h-z}{z} \frac{k_{sc}}{h-k_{sc}} \right)^Z \quad \text{for } \frac{z}{h} < 0.5 \quad (33 a)$$

$$\frac{c}{c_a} = \left(\frac{k_{sc}}{h-k_{sc}} \right)^Z \exp[-4Z(z/h-0.5)] \quad \text{for } \frac{z}{h} \geq 0.5 \quad (33 b)$$

where c_a is the reference concentration near the bottom ($z = k_{sc}$) that van Rijn (1984 b) matches with the bedload concentration, so that:

$$c_a = 0.015 \frac{d_{50}}{k_{sc}} \frac{T^{1.5}}{d_0^3} \quad (34)$$

and Z is the Rouse parameter quantifying gravity and turbulence opposite actions on the vertical adjustment of sediment particles:

$$Z = \frac{w_f}{\beta k u_* c} \quad (35)$$

where β is the factor quantifying the difference in the diffusion of fluid particles and sediment particles. According to van Rijn (1984 b), this factor is represented by:

$$\beta = 1 + 2 (w_f/u_* c)^2 \quad (36)$$

with an allowed maximum value $\beta_{max} = 1.5$ (van Rijn, personal communication).

The constant 0.015 in equation (34) is determined experimentally for a set of particle size $180 \mu m < d_{50} < 700 \mu m$.

The introduction of the fluid velocity and concentration profiles (equations 32-33) in equation (31) leads to the

following expression for the suspended load transport:

$$q_s = \frac{u_* c_a}{k} \left(\frac{k_{sc}}{h-k_{sc}} \right)^Z \left[\int_{k_{sc}}^{0.5h} \left(\frac{h-z}{z} \right)^{Z'} \ln \left(\frac{z}{k_{sc}/30} \right) dz + \int_{0.5h}^h \exp[-4Z'(z/h-0.5)] \ln \left(\frac{z}{k_{sc}/30} \right) dz \right] \quad (37)$$

with a modified Rouse parameter Z' corrected to take into account hindered settling effects and turbulence damping effects for high concentrations [$c > 0.001$ (van Rijn, 1984 b)]:

$$Z' = Z + 2.5 \left(\frac{w_f}{u_* c} \right)^{0.8} \left(\frac{c_a}{c_0} \right)^{0.4} \quad (38)$$

Equation (37) is solved numerically and the total load transport is equal to:

$$q = q_b + q_s \quad (39)$$

Numerical results for the sediment transport rates calculated by the different models at selected sites for the above chosen tidal current field are presented in Table 7. Figure 7 shows the different predicted sediment transport vector fields. Ackers and White's (1973) model results in sediment transport vectors comparatively very low ($10^{-8} \text{ m}^2 \text{ s}^{-1}$) in the inner central part of Wissant Bay and becoming larger off Cape Gris-Nez ($0.6 \cdot 10^{-5} \text{ m}^2 \text{ s}^{-1}$), in the sand-waves subsector ($0.5 \cdot 10^{-4} \text{ m}^2 \text{ s}^{-1}$) and in the sand ribbons and furrows subsector ($0.65 \cdot 10^{-4} \text{ m}^2 \text{ s}^{-1}$) located in the northeastern part of the study area. We can also notice that no sediment transport occurs in the inner western part of Wissant Bay where the initiation criterion is not reached (Fig. 7 a).

The results of Engelund and Hansen's (1967) model (Fig. 7 b) are slightly higher than those calculated from Ackers and White's (1973) model. Notice that due to the absence of threshold criterion, sediment transports occur in the inner western part of Wissant Bay characterized by very

Table 7

Sediment transport rates (in $\text{m}^2 \text{ s}^{-1}$) predicted fifteen minutes after high tide at Calais at different sites by the different models given by Ackers and White (1973), Engelund and Hansen (1967), van Rijn (1984 a; b) and Meyer-Peter and Müller (1948).

Transports sédimentaires instantanés (en $\text{m}^2 \text{ s}^{-1}$) prédits à PM à Calais + 15 mn aux différents points par les modèles de Ackers et White (1973), Engelund et Hansen (1967), van Rijn (1984 a ; b) et Meyer-Peter et Müller (1948).

site	Ackers & White's model (total load)	Engelund & Hansen's model (total load)	van Rijn's model (bedload)	van Rijn's model (suspended load)	van Rijn's model (total load)	Meyer-Peter & Müller's model (bedload)
B6	0.140e-08	0.693e-06	0.	0.	0.	0.678e-07
B10	0.141e-05	0.504e-05	0.556e-06	0.174e-05	0.230e-05	0.201e-05
C1	0.205e-05	0.614e-05	0.604e-06	0.153e-05	0.214e-05	0.228e-05
C4	0.461e-06	0.319e-05	0.129e-06	0.494e-06	0.623e-06	0.107e-05
C11	0.254e-04	0.305e-04	0.994e-05	0.122e-04	0.221e-04	0.109e-04
D6	0.188e-05	0.459e-05	0.757e-06	0.914e-06	0.167e-05	0.124e-05
E2	0.576e-05	0.856e-05	0.327e-05	0.518e-05	0.845e-05	0.392e-05
E5	0.144e-05	0.465e-05	0.109e-03	0.	0.109e-03	0.
E7	0.607e-05	0.823e-05	0.203e-05	0.220e-05	0.423e-05	0.291e-05
E12	0.660e-04	0.720e-04	0.220e-04	0.367e-04	0.587e-04	0.195e-04
F3	0.158e-04	0.190e-04	0.743e-05	0.134e-04	0.208e-04	0.801e-05
F6	0.834e-05	0.126e-04	0.290e-05	0.609e-05	0.898e-05	0.421e-05

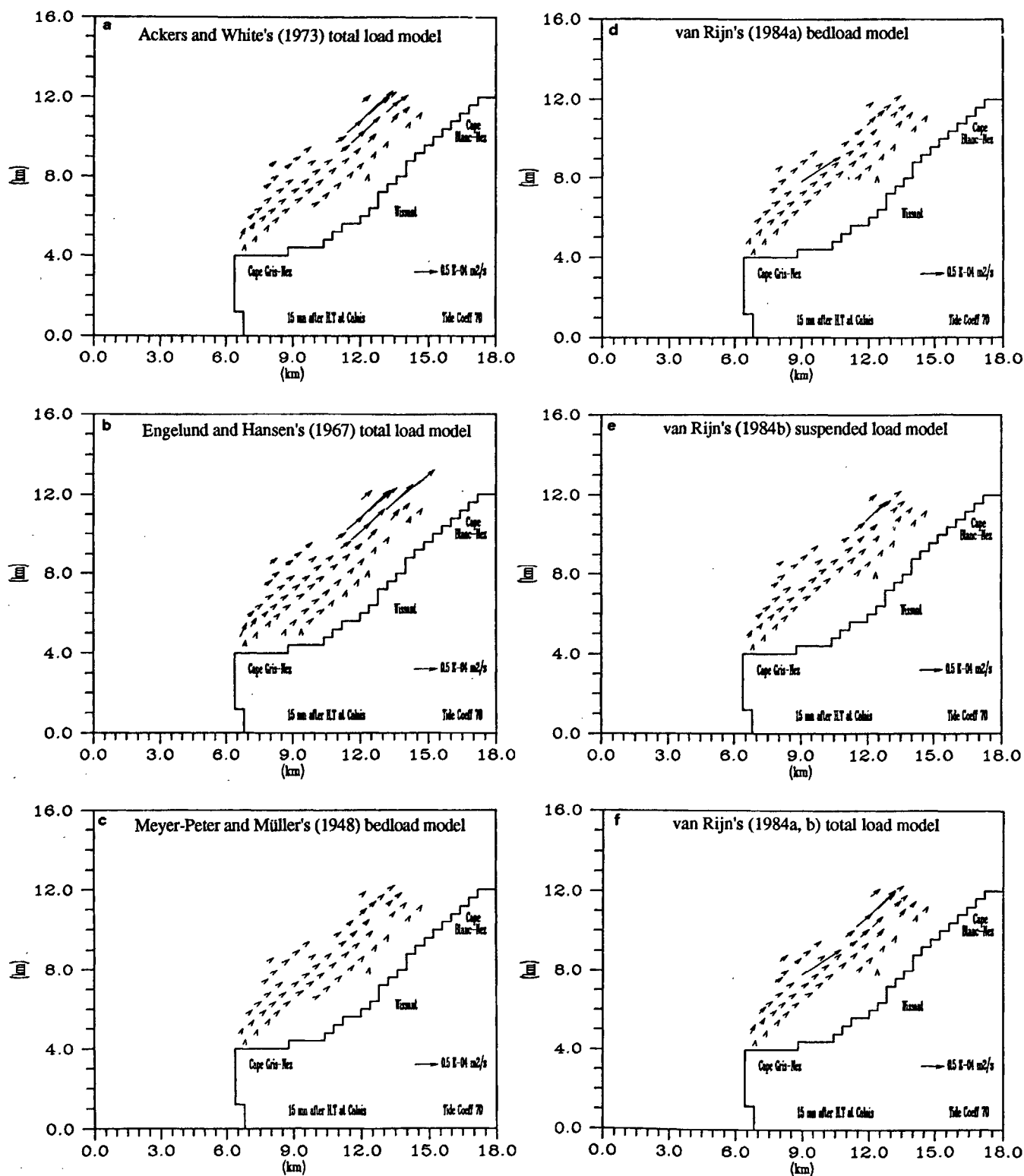


Figure 7

Sediment transport vectors predicted by: a) Ackers and White's (1973) total load model; b) Engelund and Hansen's (1967) total load model; c) Meyer-Peter and Müller's (1948) bedload model; d) van Rijn's (1984 a) bedload model; e) van Rijn's (1984 b) suspended load model; and f) total load model for the tidal velocity field depicted on Figure 6.

Vecteurs de transport sédimentaire prédits par : a) le modèle de Ackers et White (1973) ; b) le modèle de Engelund et Hansen (1967) ; c) le modèle de transport en charriage de van Rijn (1984 a) ; e) le modèle de transport en suspension de van Rijn (1984 b) ; f) le modèle de transport total de van Rijn (1984 a ; b) pour le champ des courants présenté à la figure 6.

low fluid velocities. We point out that these transport rates are extremely weak (lower than $10^{-7} \text{ m}^2 \text{ s}^{-1}$).

The application of van Rijn's (1984 *a*; *b*) model leads to total sediment transport rates that are slightly lower than those predicted by Ackers and White's (1973) model (Fig. 7 *f*). Locally higher transport rates occur in the intermediate sector. Comparison of suspended load and bedload transport rates establishes that in most cases the larger mode of transport is of a suspended load type (Fig. 7 *d*; *e*). An exception is provided by a point (E5) situated in the sand ribbons and furrows subsector. At this point, van Rijn's (1984 *a*; *b*) model predicts a strong bedload transport ($0.109 \cdot 10^{-3} \text{ m}^2 \text{ s}^{-1}$) and no suspended load transport. A close examination of the sediment shows that it is composed of a significant biogenic (shell) fraction (the percentage of CaCO_3 is equal to 62.5) determining large values of d_{35} , d_{50} and d_{65} . This sediment size is out of the range of sizes used to evaluate the constant in equation (34). Moreover, we must point out that the transportation of this kind of biogenic sediments is poorly described by the modelling procedure described herein, which focuses on sandy sediments. Consequently, this local result has to be considered very carefully. Bedload sediment transport rates predicted by van Rijn's (1984 *a*) model appear to be in reasonable agreement with those predicted by the well-known Meyer-Peter and Müller's (1948) model (Fig. 7 *c*). Concerning the initiation of sediment transport, the threshold criteria used by van Rijn (1984 *a*; *b*; 1989) lead to results very similar to those of Ackers and White (1973) results: incipient motion actually does not occur in the inner western Wissant Bay.

Calculation of the net volume of sediment transported over a semidiurnal tidal cycle

The modelling procedure is now extended to compute the volume of sediment transported during a semi-diurnal tidal cycle. This cycle is schematized by a series of twelve consecutive steps of one hour ending with a half-hour step. During each step, the flow field and the sediment transport rates field are assumed to be constant. The computation of the volume of sediment transported per tidal cycle at each point is given by:

$$\bar{Q} = \sum_{i=1}^{12} 3600 \bar{q}_i + 1800 \bar{q}_{13} \quad (40)$$

where subscript *i* refers to the *i*th step.

Figure 8 shows the net volume of sediment transported over a tidal cycle (mean tide condition) predicted by the different models. Except in a few sites located in the intermediate sector, a fairly good agreement appears between the different models. We note an almost general net transport toward the northeast (flood-dominated system) in the outer part of Wissant Bay and in the northeast part of the study area. This pattern is altered by a weak sediment recirculation in the inner western part of Wissant Bay. This local

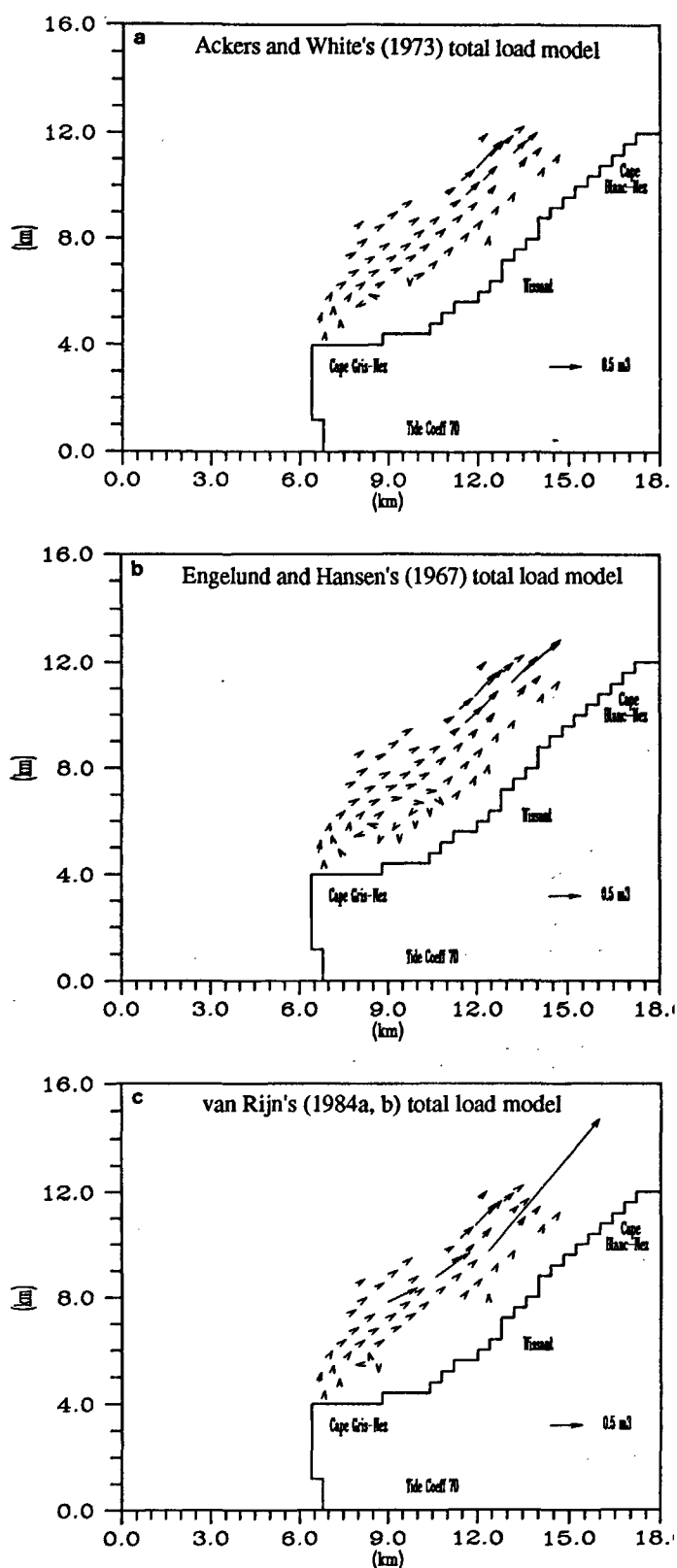


Figure 8

Net volumes of sediment transported over a mean tide cycle predicted by: a) Ackers and White's (1973) total load model; b) Engelund and Hansen's (1967) total load model; c) van Rijn's (1984 *a*; *b*) total load model.

Volumes de sédiments transportés au cours d'un cycle de marée moyenne prédits par : a) le modèle de Ackers et White (1973) ; b) le modèle de Engelund et Hansen (1967) ; c) le modèle de transport total de van Rijn (1984 *a* ; *b*).

feature situated in the Banc à la Ligne area is particularly obvious from the simulation by Engelund and Hansen's (1973) model which has no threshold criterion. Such a feature is associated to the eddy character of the tidal flow due to the advection of vorticity generated near Cape Gris-Nez. This is consistent with the mechanism of sand bank formation proposed by Pingree (1978) and Pingree and Maddock (1979). The predicted directions of sediment movement agree fairly well with those inferred from sedimentological data (*e.g.*, sand-wave alignment and asymmetry, sand ribbon orientation and obstacle marks; see Augris *et al.*, 1990; Beck *et al.*, 1991) and radioactive tracing experiments (Hoslin, 1987; Beck *et al.*, 1991).

SUMMARY AND CONCLUSIONS

Our purpose was to develop a model of tidally-induced hydro-sedimentary processes in a coastal boundary zone from a previously existing high resolution two-dimensional tidal flow model (Nguyen and Ouahsine, 1992).

Due to the multiplicity and the complexity of the problems addressed, we focused our effort on a didactic presentation of the modelling procedure. Such an approach is expected to permit the definition of a strategy founded on a hierarchization of problems to be treated in the future.

The modelling procedure consists in a series of submodels successively quantifying the shear stress applied on sediment particles, the initiation of the movement of particles and the pick-up (entrainment) processes at the bed, the ripple formation, the roughness and the shear stress related to these bedforms, as well as the sand-waves, and finally the instantaneous and tidally-averaged sediment transport rates.

The model has been applied in the tide-dominated coastal zone of Cape Gris-Nez and Cape Blanc-Nez, located in the southern part of the Dover Strait. This area was subject to a sedimentary survey. Even though the quantitative description of a number of physical phenomena involved in hydro-sedimentary processes in shallow tidal area is still subject to doubt, the model suggests:

1) a spatial variability of hydro-sedimentary processes which responds to the spatial variability of hydrodynamics

and substratum characteristics. This conclusion stresses the need to master the modelling input parameters related to sedimentology in a broad sense. At the present stage reported here, we are aware that gaps exist with regard to the substratum vertical structuration and the sedimentary environment of samples. Complementary efforts will have to be made, first in order to appreciate the representativeness of samples, especially in potentially heterogeneous regions such as those exhibiting sand ribbons, furrows and waves; and second in order to estimate the actual behavior of locally abundant shelly sediments.

2) coherent sediment transport rates predicted by the different models. Ackers and White's (1973) model predicts sediment transport rates that appear to be slightly lower than those predicted by Engelund and Hansen (1967) and slightly higher than those predicted by van Rijn (1984 *a; b*). Considering the numerous simplifications needed in modelling procedures, these differences remain weak.

3) a quasi-generalized predicted predominance of suspended load transport over bedload transport in the area under investigation.

4) a flood-dominated net sediment transport pattern altered by a weak recirculation in the western part of Wissant Bay (Banc à la Ligne area).

Although this paper focuses on modelling, it is stressed that progress can only be made by concurrently performing *in situ* field studies (*e.g.*, sampling of high-density and high-frequency, deployment of sediment traps and high-frequency sediment flux meters) and numerical modelling.

Acknowledgements

The work presented herein was done in the framework of the DYSCOP programme (Dynamique du Système Côtier du Pas-de-Calais) funded by the Nord-Pas de Calais Regional Council, the CNRS and the French National Education Ministry (contract DYSCOP-USTL-2143-RO4). The early version of the manuscript has benefited from useful comments provided by Dr. L.C. van Rijn (Delft Hydraulics and University of Utrecht).

REFERENCES

- Ackers P. and W.R. White (1973) Sediment transport: new approach and analysis. *J. Hydraul. Div., Am. Soc. Civ. Engrs*, **99**, 2041-2060.
- Allen J.R.L. (1963) Asymmetrical ripple marks and the origin of water-laid closets of cross-strata. *Geol. J.*, **3**, 187-236.
- Augris C., P. Clabaut, S. Dewez, J.-P. Auffret and C. Beck (1987 *a*) Carte des sédiments superficiels au large de Boulogne-sur-Mer. Publication Région Nord-Pas-de-Calais, IFREMER, Université de Lille, 17 pp.
- Augris C., O. Vicaire, P. Clabaut and H. Chamley (1987 *b*) Carte des sédiments superficiels au large de Calais-Dunkerque. Publication Région Nord-Pas-de-Calais, IFREMER, Université de Lille, 19 pp.
- Augris C., P. Clabaut and O. Vicaire (1990) Le domaine marin du Nord-Pas-de-Calais: nature, morphologie et mobilité des fonds. Publication Région Nord-Pas-de-Calais, IFREMER, 96 pp.
- Bagnold R.A. (1956) Flow of cohesionless grains in fluids. *Phil. Trans. R. Soc.*, **A249**, 235-297.

- Bagnold R.A.** (1966) An approach to the sediment transport problem from the general physics. *U.S. Geol. Surv., Prof. Pap.*, 422-I, 37 pp.
- Beck C., P. Clabaut, S. Dewez, O. Vicaire, H. Chamley, C. Augris, R. Hoslin and A. Caillot** (1991) Sand bodies and sand transport paths at the English Channel-North Sea border: morphology, hydrodynamics and radioactive tracing. *Proceedings of the International Colloquium on the environment of epicontinental seas, Lille, France, 20-22 March 1990, Oceanologica Acta, sp. issue No.11*, 111-121.
- Dyer K.H.** (1986) *Coastal and estuarine sediment dynamics*. John Wiley and Sons, New York, 342 pp.
- Einstein H.A.** (1950) The bedload function for sediment transport in open channel flows. U.S. Department of Agriculture. Soil Conservation Service, Technical Bulletin No. 1026, 70 pp.
- Engelund F.** (1965) A criterion for the occurrence of suspended load. *La Houille Blanche*, 8, 7.
- Engelund F. and E. Hansen** (1967) A monograph on sediment transport in alluvial streams. Teknisk Forlag, Copenhagen, Denmark, 62 pp.
- Hinze J.O.** (1959) *Turbulence*. McGraw-Hill Book Co., Inc., New York, 586 pp.
- Hoslin R.** (1987) Mesure par traceurs radioactifs des déplacements sédimentaires aux abords du Cap Gris-Nez. Rapport du Commissariat à l'Énergie Atomique, France, 50 pp.
- Kreplin H.P. and H. Eckelmann** (1979) Behavior of the three fluctuating velocity components in the wall region of a turbulent channel flow. *Phys. Fluids*, 22, 7, 1233-1239.
- Meyer-Peter E. and R. Müller** (1948) Formulas for bedload transport. *Proceedings of the 2nd Congress IAHR*, 39-64.
- Middleton G.V.** (1976) Hydraulic interpretation of sand distributions. *J. Geol.*, 84, 405-426.
- Nguyen K. D. and A. Ouahsine** (1992) Modèle numérique 2-D de la circulation générale dans la zone littorale du Nord-Pas de Calais. Rapport DYSCOP, 27 pp.
- O'Connor B.A.** (1991) Suspended sediment transport in the coastal zone. *Proceedings of the International Symposium on the Transport of suspended sediments and its mathematical modelling, Florence, Italy*, 17-63.
- Pingree R.D.** (1978) The formation of the Shambles and others Banks by tidal stirring of the seas. *J. mar. biol. Ass. U.K.*, 58, 211-226.
- Pingree R.D. and L. Maddock** (1979) The tidal physics of headland flows and offshore tidal bank formation. *Mar. Geol.*, 33, 269-289.
- Raudkivi A.J.** (1976) *Loose Boundary Hydraulics*. Pergamon Press, 397 pp.
- van Rijn L.C.** (1981) Computation of bedload concentration and bedload transport. Delft Hydraulics Laboratory, Research Report S 487-I, Delft, The Netherlands.
- van Rijn L.C.** (1982) Equivalent roughness of alluvial bed. *J. Hydraul. Div., Am. Soc. civ. Engrs*, 108, 10, 1215-1218.
- van Rijn L.C.** (1984 a) Sediment transport. Part I: Bedload transport. *J. Hydraul. Div., Am. Soc. civ. Engrs*, 110, 10, 1431-1456.
- van Rijn L.C.** (1984 b) Sediment transport. Part II: Suspended load transport. *J. Hydraul. Div., Am. Soc. civ. Engrs*, 110, 11, 1494-1502.
- van Rijn L.C.** (1984 c) Sediment pick-up functions. *J. Hydraul. Div., Am. Soc. civ. Engrs*, 110, 10, 867-874.
- van Rijn L.C.** (1986) Applications of sediment pick-up function. *J. Hydraul. Div., Am. Soc. civ. Engrs*, 112, 9, 867-874.
- van Rijn L.C.** (1989) Handbook of sediment transport by currents and waves. Delft Hydraulics Laboratory, Report H 461, Delft, The Netherlands.
- Salomon J.-C. and M. Breton** (1991) Courants résiduels de marée dans la Manche. *Proceedings of the International Colloquium on the environment of epicontinental seas, Lille, France, 20-22 March 1990, Oceanologica Acta, sp. issue No.11*, 47-53.
- Shields A.** (1936) Anwendung der Ähnlichkeitsmechanik und der Turbulenzforschung auf die Geschiebebewegung. Berlin Preuss Versuchsanstalt für Wasser, Erd und Schiffbau, 26, 1-26.
- Shinohara K. and T. Tsubaki** (1959) On the characteristics of sand-waves formed upon beds of the open channels and rivers. Kyushu University. *Repts Res. Inst. appl. Mech.*, 7, 25.
- Sleath J.F.A.** (1984) *Sea-bed mechanics*. Wiley Ocean Engineering Series, New York, USA, 335 pp.
- Werner F.E. and D.R. Lynch** (1987) Field verification of wave equation tidal dynamics in the English Channel and southern North Sea. *Adv. Wat. Resour.*, 12, 184-193.
- White W.R., H. Milli and A.D. Crabbe** (1975) Sediment transport theories: a review. *Proc. Inst. Civ. Engng, Part 2*, 59, 265-292.
- Wooding R.A., E.F. Bradley and J.K. Marshall** (1973) Drag due to regular arrays of roughness elements of varying geometry. *Boundary-layer Met.*, 5, 285-308.
- Yalin M.S.** (1985) On the determination of ripple geometry. *J. Hydraul. Div.*, 111, 8, 1148-1155.